Stem Cell Reports, Volume *10*

Supplemental Information

Astrocytes Attenuate Mitochondrial Dysfunctions in Human Dopaminergic Neurons Derived from iPSC

Fang Du, Qing Yu, Allen Chen, Doris Chen, and Shirley ShiDu Yan

Supplemental Figures and Legends

Supplementary Figure S1.

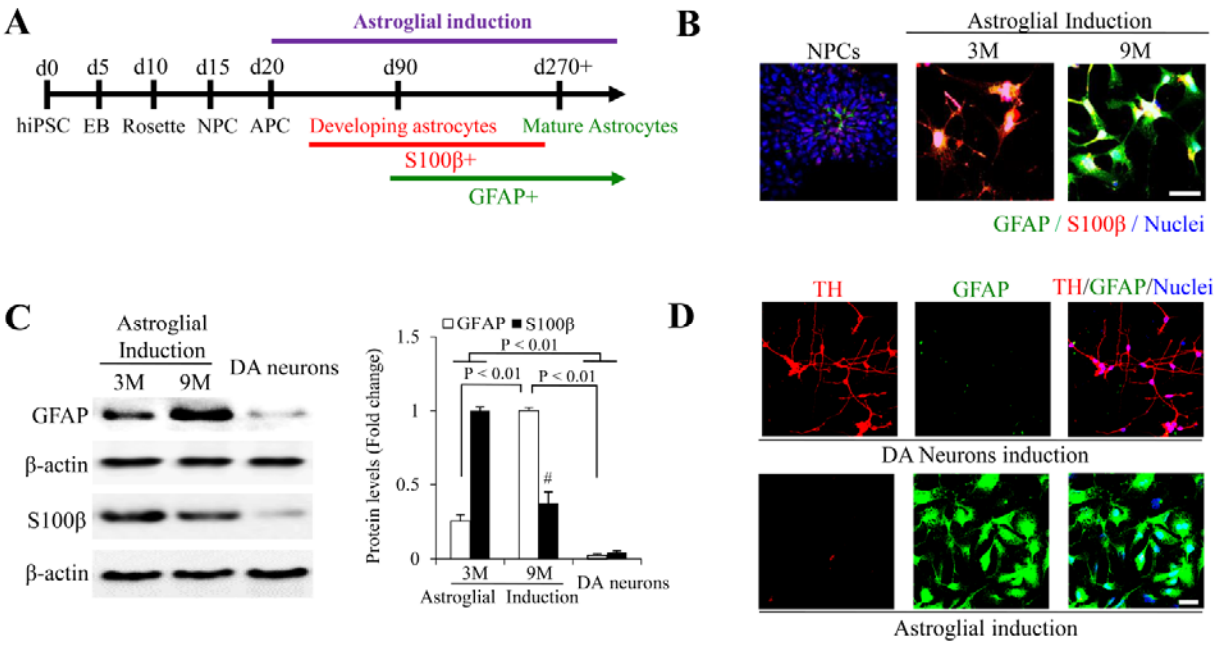

Figure S1 (Related to Figure 1: Differentiation and development of hiPSC line-induced human astrocytes). Differentiation of hiPSCs BM2-3 lines into astrocytes. (**A**) A schematic representation of processes of differentiation of human bone marrow fibroblast-derived hiPSCs BM2-3 into astroglial progenitors (S100β+) and mature astrocytes (GFAP+). (**B**) Immunocytochemistry of GFAP (Marker for definitive astrocytes, green) and S100β (Marker for astroglial progenitor, red) in neural progenitor cells (NPCs), astroglial progenitor (3 months with astroglial induction) and mature astrocytes (9 months with astroglial induction). Nuclei were stained by DRAQ5 (5 μM, Cell Signaling). Scale bar, 50 μm. (**C**) immunoblotting analyses to detect GFAP and S100β in astroglial and mature astrocytes in comparison with hiPSCs induced DA neurons. #P < 0.05 vs. 3-month astrocytes and DA neurons (Black bars, S100β). (**D**) Immunocytochemistry of TH (red) and GFAP (green) in mature DA neurons (up panel) and

mature astrocytes (bottom panel). Nuclei were stained by DRAQ5. Scale bar, 50 μm. For (**C**), statistical analysis was performed using Statview software (SAS Institute, Version 5.0.1). One-way ANOVA was used for repeated measure analysis, followed by Fisher's protected least significant difference for post hoc comparisons. Data are presented as mean ± SEM. n = 3 independent experiments.

Supplementary Figure S2.

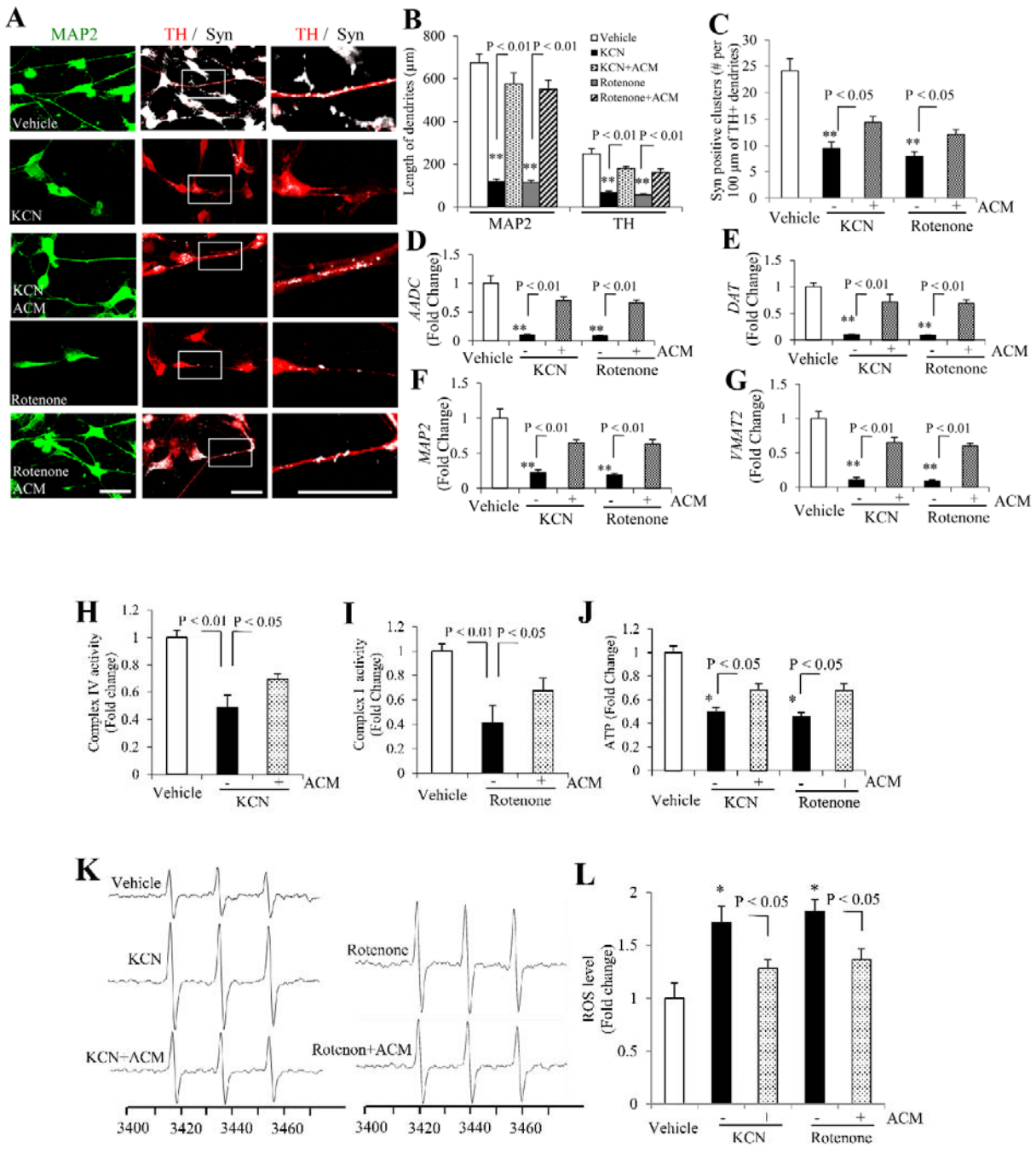

Figure S2 (Related to Figure 2: Astrocyte co-culture rescues differentiation of hiPSC line-induced human DA neurons under KCN or rotenone treatment, and Figure 3. Effect of astrocyte co-culture on mitochondrial functions in hiPSC line-induced human DA neurons under KCN or rotenone treatment). Astrocyte conditioned medium (ACM) rescues differentiation impairment and mitochondrial dysfunction of hiPSC line-induced human DA neurons under KCN or rotenone treatment. The effects of ACM on the differentiation ability and mitochondrial functions in hiPSC line-induced human DA neurons under KCN or rotenone treatment were also observed and compared to the co-culture system. (**A**) Representative images for immunostaining of MAP2 (green), TH (red) and Syn (White, color changed from far red) in induced DA neurons treated with KCN or rotenone with or without ACM cotreatment. (**B**) Quantification of neuronal process length of MAP2-positive neurons and TH-positive DA neurons using NIH Image J program. (**C**) Quantification of numbers of Syn-positive clusters along the branches of hiPSC-derived DA neurons (TH-positive dendrities). (**D-G**) Quantitative RT-PCR results of the gene expression in DA neurons with the above treatments. Scale bars = 25 μm in **A**. Complex IV (**H**) and I (**I**) activity and ATP levels (**J**) were determined in hiPSC-derived DA neurons treated with KCN or rotenone with or without ACM cotreatment. (**K-L**) Assessment of intracellular ROS levels measured by EPR spectroscopy. Representative images for EPR are shown in **K**, and quantifications are shown in **L**. For (**B-J** and **L**), statistical analysis was performed using Statview software (SAS Institute, Version 5.0.1). One-way ANOVA was used for repeated measure analysis, followed by Fisher's protected least significant difference for post hoc comparisons. Data are presented as mean ± SEM. n = 3 independent experiments, with 12 cells quantified per experiment in (**B-C**). n = 3 independent experiments in **D-J** and **L**; mean ± SEM.

Supplementary Figure S3.

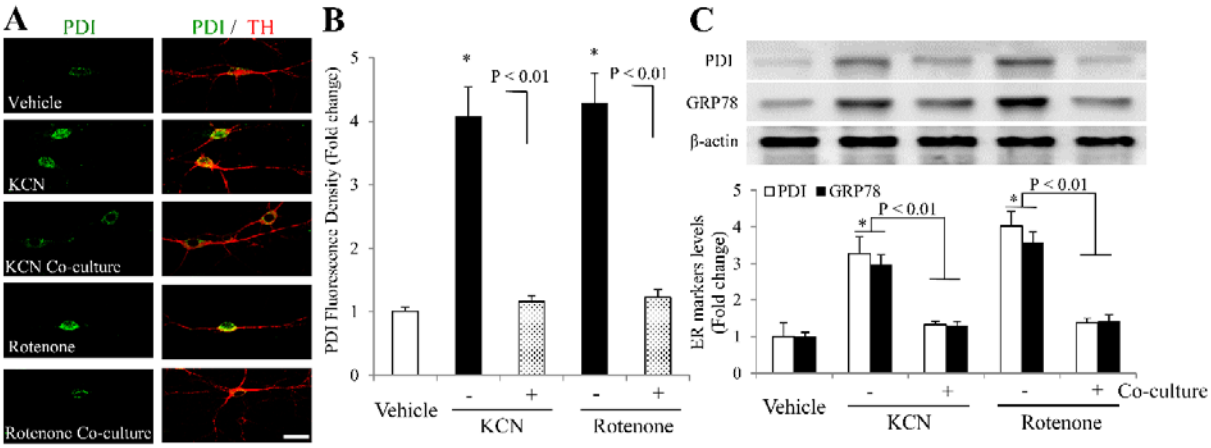

Figure S3 (Related to Figure 3. Effect of astrocyte co-culture on mitochondrial functions in hiPSC line-induced human DA neurons under KCN or rotenone treatment). Astrocyte co-culture rescues ER stress in differentiation of hiPSC line-induced human DA neurons under KCN or rotenone treatment. Besides mitochondrial dysfunction (**Figure 3**), long-term application of low doses of KCN and rotenone also induced ER stress in hiPSC-induced DA neurons, whereas astrocyte co-culture rescued both mitochondrial dysfunction (**Figure 3**) and ER stress. (**A**) Immunocytochemistry of a luminal endoplasmic reticulum (ER) protein, PDI (Protein disulfide isomerase) and TH (red) in mature DA neurons, and (**B**) bar graph shows the quantification of fluorescence density of PDI in DA neurons using NIH Image J program. (**C**) Immunoblotting analyses to detect PDI and GRP78 (Glucose-regulated protein 78, used as a marker of ER stress) in hiPSC-induced DA neurons. *P < 0.01 vs. vehicle group (**B-C**).

Supplementary Video S1. (Related to Figures 4B-F). Mitochondrial movement in the neurites of hiPSC-derived DA neurons with different treatments. Videos S1A-E: mitochondrial movement in the neurites of hiPSC-derived DA neurons with vehicle treatment

(**Video S1A**); KCN treatment (**Video S1B**); rotenone treatment (**Video S1C**), and KCN (**Video S1D**) or rotenone (**Video S1E**) treatment with astroglial co-culture.

Supplemental Experimental Procedures

Formation of embryoid bodies and induction of rosette

Feeder-free iPSCs were dissociated with TryplE and seeded onto AggreWell™800 plate (10,000 cells per embryoid body; Stem Cell Technologies) in E8 media supplemented with 10 μM ROCK inhibitor Y27632 for the first 24 h; we changed 75% of the media daily with STEMdiff™ Neural Induction Medium (NIM, Stem Cell Technologies). Embryoid bodies were harvested after 5 days and plated onto poly-L-ornithine/laminin (PLO/L, Sigma) coated plates. 1-2 day(s) after attachment, prominent neural rosette structures were visible inside the attached neural aggregates. Rosettes were formed by cells expressing proteins characteristic of progenitor markers of PAX6 and Ki67 (Fang et al., 2016a; Fang et al., 2016b).

Isolation of stem/progenitor cells and differentiation of DA neurons

We followed the differentiation protocol (Hartfield et al., 2014) with some modifications. Briefly, stem/progenitor cells from neuronal rosette clusters were isolated using Neural Rosette Selection Reagent (Stem Cell Technologies) 5 days after incubation in NIM. Detached cells were collected and plated onto poly l Ornithine/Laminin (PLO/L) coated 6-well plates for Western blot analysis and complex activities measurement (2×10^4 cells per well), 12-well plates for co-culture system (1×10^4 cells per well), or coverslips for immunocytochemistry and electrophysiology (5×10^3 cells per coverslip). Neural progenitor cells (NPCs) were cultured in neural expansion medium (DMEM/F12 supplemented with 1 × B27 and N2 [Life technologies], fibroblast growth factor-8a [FGF8a, 100 ng/ml, Life technologies], sonic hedgehog [SHH C25II,

200 ng/ml, Life technologies]; Heparin [2 μg/ml, Life technologies] and 1× non-essential amino acids [NEAA, Life technologies] for 5 days and finally in DA neuronal differentiation medium (Neurobasal medium supplemented with L-glutamine [2 mM, Life technologies], 1× B27 and N2 supplements, Brain-derived neurotrophic factor [BDNF, 25 ng/ml], glial-derived neurotrophic factor [GDNF, 20 ng/ml], N6,29-O-dibutyryladenosine 39,59-cyclic monophosphate sodium salt [dCAMP, 100 μM; Sigma] and ascorbic acid [200 μM, Sigma]).

Astroglial differentiation

Astroglial progenitors were differentiated from iPSCs as previously described with some modifications (Krencik et al., 2011; Williams et al., 2014). Briefly, iPSCs were first differentiated to rosettes (Day 10). After cultured in neural expansion medium for 5 days (Day 10-15) and another 5 days for astroglial progenitor cells (APCs) differentiation in an astroglial expansion medium (DMEM/F12 supplemented with N2; Heparin [2μg/ml] and 1× NEAA; Day 15-20), the medium was switched to astroglial progenitor media (APM): astroglial expansion medium with the addition of 10 ng/ml EGF (Pepro-Tech) and 10 ng/ml recombinant human FGF2. From Day 21, these APCs were passaged with Accutase (Life technologies) every 14 days, and were plated at a density of 5×10^4 cells per well in astroglial media (AM): APM with the addition of ciliary neurotrophic factor (CNTF). Terminal differentiated astrocytes were derived from 3 months to 9 months by the removal of the growth factors (EGF and FGF2) in AM.

For astroglial conditioned media (ACM) collection, 2.5×10^4 astrocytes per well were first seeded on the PLO/L coated 12-well plate and allowed to grow for 5 days. On day 6, AM was changed to DA neuronal differentiation medium (500 μl). The medium (ACM) was centrifuged to pellet debris and collected every 2 days, and was used to treat NPC and DA neurons, with or without the presence of mitochondrial inhibitor/ toxin (**Figure 1A**).

Immunoblotting analysis

NPCs, DA neurons, astroglial progenitor and astrocytes were washed with ice-cold PBS and proteins extracted with 150μl of lysis buffer. After centrifugation at 12,000 × g for 10 min at 4°C, we collected the supernatant and determined protein concentrations; we boiled 30 μg proteins in protein loading buffer for 5 min, separated the proteins on a 10% SDS polyacrylamide gel, and subsequently transferred to nitrocellulose membranes. Nonspecific binding was inhibited by incubation in TBST (20 mM Tris-buffered saline with 0.1% Tween 20, pH 7.5) containing 5% nonfat dried milk for 1 hour at room temperature. Membranes were incubated with the following primary antibodies: rabbit anti-S100β (1:500, Abcam, ab52642-100), mouse anti-GFAP antibody (1:3000, Cell signaling, #3670), rabbit anti-TH (1:2000, Chemicon, #657012), mouse anti-PDI IgG (1: 10,000, StressGen, # SPA-891) and rabbit anti-GRP78 (1:5000, StressGen, # SPA-826) overnight at 4°C. After three washes with TBST, membranes were incubated for 2 h with horseradish (HRP)-conjugated secondary antibodies (Pierce Chemical Company, USA) and developed using enhanced chemiluminescence (ECL Amersham Biosciences, England). To ensure equal protein loading of the samples, the same membrane was probed with anti-mouse β-actin monoclonal antibody (Sigma-Aldrich, MO) at a 1: 10,000 dilution.

Immunocytochemistry

The induced DA neurons, NPCs, or the astrocytes, were fixed with 4% ice-cold paraformaldehyde for 5 min and then permeabilized with PBS containing 0.1% Triton and 5% goat serum for 1 h followed by incubation with the following primary antibodies: rabbit anti-S100β (1:500, Abcam, ab52642-100) and mouse anti-GFAP antibody (1:3000, Cell signaling, #3670); rabbit anti-TH (1:2000, Chemicon, #657012) and mouse anti-Syn IgG (1:1000,

chemicon, #MAB5258); rabbit anti-TH (1:2000, Chemicon, #657012) and mouse anti-PDI IgG (1:5000, StressGen, # SPA-891); or rabbit anti-MAP2 (1:5000, Thermo Fisher, # PA517646) at 4°C for 16 h. Cells were incubated with Alexa Fluor 488-conjugated goat anti-mouse IgG and 594 goat anti-rabbit IgG (1: 1000, Invitrogen) or anti-rabbit IgG and 488 goat anti-mouse IgG (1: 1000, Invitrogen) for 1 h at room temperature. After washing with PBS, neurons were covered with Vectashield mounting medium (H-1000, Vector Laboratories). Images were acquired (equal exposure for all groups) using confocal microscopy (Leica) and analyzed using the Universal Metamorph Image Program.

We measured synaptic density of cultured neurons by counting the number of synaptophysin-positive clusters in neuronal dendrites and puncta per 100 microns of TH positive dendrite (presented as the number of synaptophysin clusters per 100 microns of dendrite) and calculated by dividing the length of the TH+ dendrites. Soma size analysis of DA neurons was measured in TH-positive neurons from 30 randomly selected fields using ImageJ software.

Real-time PCR measurement

RNA was extracted identified cells by using TRIzol reagents (Invitrogen, Carlsbad, CA, USA) according to the manufacturer's protocol as described in our previous study (Fang et al., 2015). cDNA was directly preformed using TaqMan reverse transcription reagents kit (Applied Biosystems, Foster City, CA, USA). Total RNA (1 μg) was used for the synthesis of cDNA with TaqMan Reverse Transcription Reagents kit (Roche Applied Biosystems). Real time-PCR was performed on an ABI Prism 7900 Sequence Detection System (Applied Biosystems) with TaqMan PCR Master Mix. Semi-quantitative PCR was performed in the GeneAmp PCR System 2720 (Applied Biosystems), and the same volume of reaction products are electrophoresed on an agarose gel. The sequences of the primers were EN1 (Hs00154977_m1, Thermo Fisher), OTX2

(Hs00222238_m1, Thermo Fisher), FOXA2 (Hs00232764_m1, Thermo Fisher), map2 (Hs00258900_m1, Thermo Fisher), DDC (AADC) (Hs01105048_m1, Thermo Fisher), SLC18A2 (VMAT2) (Hs00996835_m1, Thermo Fisher), LMX1A (Hs00892663_m1, Thermo Fisher), SLC6A3 (DAT) (Hs00997374_m1, Thermo Fisher), ZBTB16 (PLzf) (Hs00957433_m1, Thermo Fisher), DACH1 (Hs00362088_m1, Thermo Fisher).

Measurement of respiratory chain complex enzyme activities and ATP levels

Enzyme activities in complex I (NADH-ubiquinonereductase), complex IV (cytochrome c oxidase, CcO), and ATP levels were determined as described previously (Gan et al., 2014a). The reaction was then initiated by the addition of 50 µl of ferrocytochrome substrate solution (0.22 mM) and changes in absorbance of cytochrome c at 550 nm were measured using a Shimadzu (Kyoto, Japan) UV1200 spectrophotometer. Activity is expressed as micromols of cytochrome oxidized per min^{-1} mg^{-1} protein using an extinction coefficient of 18.64 mM^{-1} cm^{-1}.

ATP levels were determined using an ATP Bioluminescence Assay Kit (Roche) following the manufacturer's instructions (Du et al., 2008; Du et al., 2010). Briefly, cells were harvested using the provided lysis buffer, incubated on ice for 15 minutes, and centrifuged at 13,000g for 10 minutes. ATP levels were measured using a Luminescence plate reader (Molecular Devices) with an integration time of 10 seconds.

Determination of mitochondrial ROS generation with MitoSox Red

Differentiated neuronal cells were seeded at low density onto Lab-Tek eight-well chamber slides (10,000 cells /well). Mitochondrial ROS generation was determined using MitoSox Red (Invitrogen), a unique fluorogenic dye highly selective for detection of superoxide production in live cell mitochondria (Gan et al., 2014a; Gan et al., 2014b; Iuso et al., 2006; Polster et al., 2014; Xu and Chisholm, 2014). Cells were incubated with fresh medium containing 2.5 µM MitoSox

for 30 min at 37°C. To detect mitochondrial ROS in DA neurons, cells were fixed and incubated with rabbit anti-TH (1:2000, Chemicon, #657012) at 4°C for 16 h. followed by incubation with Alexa Fluor 488-conjugated goat anti-rabbit IgG (1: 1000, Invitrogen) for 1 h at room temperature. Fluorescence images were acquired on a Leica SP5 confocal microscope and analyzed using Leica LAS AF software (Leica Wetzlar). Excitation wavelengths were 543 nm for MitoSox and 488nm for TH. Fluorescent signals were quantified using NIH Image J software. We used MetaMorph (Molecular Devices) and NIH Image J software for quantification and measurement of fluorescent signals.

Evaluation of intracellular ROS levels

Intracellular ROS levels were accessed by election paramagnetic resonance (EPR) spectroscopy as described in our previous study (Fang et al., 2015; Fang et al., 2016c). CMH (cyclic hydroxylamine 1-hydroxy-3-methoxycarbonyl-2, 2, 5, 5-tetramethyl-pyrrolidine, 100μM) was incubated with cultured cells for 30 min and then washed with cold PBS. The cells were collected and homogenized with 100 μl of PBS for EPR measurement. The EPR spectra were collected, stored, and analyzed with a Bruker EleXsys 540 x-band EPR spectrometer (Billerica, MA) using the Bruker Software Xepr (Billerica, MA).

Axonal mitochondrial trafficking recording and data analysis in differentiated neuronal cells

These recordings were performed using previously reported protocols (Du et al., 2010; Guo et al., 2013). Axonal mitochondria were visualized following transfection with pDsRed2-mito (Clontech) in differentiated neuronal cells using lipofectamine LTX and plus regent (Invitrogen) according to the manufacturer's protocol. Three to four days after transfection, time-lapse recordings of labeled mitochondrial movement were acquired on a Carl Zeiss (Axiovert 200)

microscope with incubation system (PeCon) to maintain differentiated neuronal cells at 37°C during image collection. Collection of image stacks and velocity measurements were made using the AxioVision Software as previously described (Du et al., 2010; Guo et al., 2013). For standard recordings, images of mitochondria in one process per differentiated neuronal cell were collected every 3 s for 2 min. Only the proximal segment of the axon was acquired and recorded.

Mitochondria in each frame of every video recording were individually tracked using AxioVision Software and the average velocity was calculated during the 2-min recording period. The average velocity of every mitochondrion in one measured process in each cell was then averaged to obtain the average velocity for mitochondrial movement per process. In addition, the percentage of movable mitochondria, mitochondrial total traveling distance (total distance traveled irrespective of direction during the recording period), single mitochondrial length and mitochondrial density in each process were all determined according to previous studies with modifications (Gan et al., 2014a; Trimmer and Borland, 2005). Exposure periods (30–50 ms) were kept at a minimum to limit phototoxicity.

Statistical analysis

Statistical analysis was performed using Statview software (SAS Institute, Version 5.0.1). One-way ANOVA or Student's t-test was used for repeated measure analysis, followed by Fisher's protected least significant difference for post hoc comparisons. Data are presented as mean ± SEM. $P < 0.05$ was considered significant.

Supplemental References

Du, H., Guo, L., Fang, F., Chen, D., Sosunov, A.A., McKhann, G.M., Yan, Y., Wang, C., Zhang, H., Molkentin, J.D., *et al.* (2008). Cyclophilin D deficiency attenuates mitochondrial and neuronal perturbation and ameliorates learning and memory in Alzheimer's disease. Nature medicine *14*, 1097-1105.

Du, H., Guo, L., Yan, S., Sosunov, A.A., McKhann, G.M., and Yan, S.S. (2010). Early deficits in synaptic mitochondria in an Alzheimer's disease mouse model. Proceedings of the National Academy of Sciences of the United States of America *107*, 18670-18675.

Fang, D., Qing, Y., Yan, S., Chen, D., and Yan, S.S. (2016a). Development and Dynamic Regulation of Mitochondrial Network in Human Midbrain Dopaminergic Neurons Differentiated from iPSCs. Stem cell reports *7*, 678-692.

Fang, D., Wang, Y., Zhang, Z., Du, H., Yan, S., Sun, Q., Zhong, C., Wu, L., Vangavaragu, J.R., Yan, S., *et al.* (2015). Increased neuronal PreP activity reduces Abeta accumulation, attenuates neuroinflammation and improves mitochondrial and synaptic function in Alzheimer disease's mouse model. Human molecular genetics *24*, 5198-5210.

Fang, D., Yan, S., Yu, Q., Chen, D., and Yan, S.S. (2016b). Mfn2 is Required for Mitochondrial Development and Synapse Formation in Human Induced Pluripotent Stem Cells/hiPSC Derived Cortical Neurons. Scientific reports *6*, 31462.

Fang, D., Zhang, Z., Li, H., Yu, Q., Douglas, J.T., Bratasz, A., Kuppusamy, P., and Yan, S.S. (2016c). Increased Electron Paramagnetic Resonance Signal Correlates with Mitochondrial Dysfunction and Oxidative Stress in an Alzheimer's disease Mouse Brain. Journal of Alzheimer's disease : JAD *51*, 571-580.

Gan, X., Huang, S., Wu, L., Wang, Y., Hu, G., Li, G., Zhang, H., Yu, H., Swerdlow, R.H., Chen, J.X., *et al.* (2014a). Inhibition of ERK-DLP1 signaling and mitochondrial division alleviates mitochondrial dysfunction in Alzheimer's disease cybrid cell. Biochimica et biophysica acta *1842*, 220-231.

Gan, X., Wu, L., Huang, S., Zhong, C., Shi, H., Li, G., Yu, H., Howard Swerdlow, R., Xi Chen, J., and Yan, S.S. (2014b). Oxidative stress-mediated activation of extracellular signal-regulated kinase contributes to mild cognitive impairment-related mitochondrial dysfunction. Free radical biology & medicine *75*, 230-240.

Guo, L., Du, H., Yan, S., Wu, X., McKhann, G.M., Chen, J.X., and Yan, S.S. (2013). Cyclophilin D deficiency rescues axonal mitochondrial transport in Alzheimer's neurons. PloS one *8*, e54914.

Hartfield, E.M., Yamasaki-Mann, M., Ribeiro Fernandes, H.J., Vowles, J., James, W.S., Cowley, S.A., and Wade-Martins, R. (2014). Physiological characterisation of human iPS-derived dopaminergic neurons. PLoS One *9*, e87388.

Iuso, A., Scacco, S., Piccoli, C., Bellomo, F., Petruzzella, V., Trentadue, R., Minuto, M., Ripoli, M., Capitanio, N., Zeviani, M., *et al.* (2006). Dysfunctions of cellular oxidative metabolism in patients with mutations in the NDUFS1 and NDUFS4 genes of complex I. The Journal of biological chemistry *281*, 10374-10380.

Krencik, R., Weick, J.P., Liu, Y., Zhang, Z.J., and Zhang, S.C. (2011). Specification of transplantable astroglial subtypes from human pluripotent stem cells. Nature biotechnology *29*, 528-534.

Polster, B.M., Nicholls, D.G., Ge, S.X., and Roelofs, B.A. (2014). Use of potentiometric fluorophores in the measurement of mitochondrial reactive oxygen species. Methods in enzymology *547*, 225-250.

Trimmer, P.A., and Borland, M.K. (2005). Differentiated Alzheimer's disease transmitochondrial cybrid cell lines exhibit reduced organelle movement. Antioxidants & redox signaling *7*, 1101-1109.

Williams, E.C., Zhong, X., Mohamed, A., Li, R., Liu, Y., Dong, Q., Ananiev, G.E., Mok, J.C., Lin, B.R., Lu, J., *et al.* (2014). Mutant astrocytes differentiated from Rett syndrome patients-specific iPSCs have adverse effects on wild-type neurons. Human molecular genetics *23*, 2968-2980.

Xu, S., and Chisholm, A.D. (2014). C. elegans epidermal wounding induces a mitochondrial ROS burst that promotes wound repair. Developmental cell *31*, 48-60.